Contextualizing the pathology in the essential tremor cerebellar cortex: a patholog-omics approach

Elan D. Louis[1,2,3], **Chloë A. Kerridge**[4], **Debotri Chatterjee**[4], **Regina T. Martuscello**[4], **Daniel Trujillo Diaz**[1], **Arnulf H. Koeppen**[5], **Sheng-Han Kuo**[6], **Jean-Paul G. Vonsattel**[4,7], **Peter A. Sims**[8,9,10], **Phyllis L. Faust**[4]

[1]Department of Neurology, Yale School of Medicine, Yale University, 15 York Street, PO Box 208018, New Haven, CT 06520-8018, USA

[2]Department of Chronic Disease Epidemiology, Yale School of Public Health, Yale University, New Haven, CT, USA

[3]Center for Neuroepidemiology and Clinical Neurological Research, Yale School of Medicine, Yale University, New Haven, CT, USA

[4]Department of Pathology and Cell Biology, Columbia University Irving Medical Center and the New York Presbyterian Hospital, 622 West 168th Street, PH Stem 1564, New York, NY 10032, USA

[5]Research, Neurology, and Pathology Services, Veterans Affairs Medical Center and Departments of Neurology and Pathology, Albany Medical College, Albany, NY, USA

[6]Department of Neurology, College of Physicians and Surgeons, Columbia University, New York, NY, USA

[7]Taub Institute for Research on Alzheimer's Disease and the Aging Brain, Columbia University, New York, NY, USA

[8]Department of Systems Biology, Columbia University Irving Medical Center, New York, NY 10032, USA

[9]Sulzberger Columbia Genome Center, Columbia University Irving Medical Center, New York, NY, USA

[10]Department of Biochemistry and Molecular Biophysics, Columbia University Irving Medical Center, New York, NY, USA

Abstract

Several morphological changes, centered in/around Purkinje cells (PCs), have been identified in the cerebellum of essential tremor (ET) patients. These changes have not been contextualized within a broader degenerative disease spectrum, limiting their interpretability. To address this, we

compared the severity and patterning of degenerative changes within the cerebellar cortex in patients with ET, other neurodegenerative disorders of the cerebellum (spinocerebellar ataxias (SCAs), multiple system atrophy (MSA)], and other disorders that may involve the cerebellum [Parkinson's disease (PD), dystonia]. Using a postmortem series of 156 brains [50 ET, 23 SCA (6 SCA3; 17 SCA 1, 2 or 6), 15 MSA, 29 PD, 14 dystonia, 25 controls], we generated data on 37 quantitative morphologic metrics, which were grouped into 8 broad categories: (1) PC loss, (2) heterotopic PCs, (3) PC dendritic changes, (4) PC axonal changes (torpedoes), (5) PC axonal changes (other than torpedoes), (6) PC axonal changes (torpedo-associated), (7) basket cell axonal hypertrophy, (8) climbing fiber-PC synaptic changes. Our analyses used z scored raw data for each metric across all diagnoses (5772 total data items). Principal component analysis revealed that diagnostic groups were not uniform with respect to cerebellar pathology. Dystonia and PD each differed from controls in only 2/37 metrics, whereas ET differed in 21, SCA3 in 8, MSA in 19, and SCA1/2/6 in 26 metrics. Comparing ET with primary disorders of cerebellar degeneration (i.e., SCAs), we observed a spectrum of changes reflecting differences of degree, being generally mild in ET and SCA3 and more severe in SCA1/2/6. Comparative analyses across morphologic categories demonstrated differences in relative expression, defining distinctive patterns of changes in these groups. Thus, the degree of cerebellar degeneration in ET aligns it with a milder end in the spectrum of cerebellar degenerative disorders, and a somewhat distinctive signature of degenerative changes marks each of these disorders.

Keywords

Essential tremor; Cerebellum; Spinocerebellar ataxia; Parkinson's disease; Dystonia

Introduction

For many years, the pathological anatomy of essential tremor (ET) had been a mystery [29]. Postmortem studies were largely restricted to single case reports. Furthermore, qualitative rather than rigorous quantitative approaches were used, many of the "ET" cases had other neurological disorders rather than ET, and none of the studies enrolled control brains for contextual comparison [36]. In more recent postmortem studies, we and others have identified a growing number of morphological changes in the ET cerebellum, predominantly centered in/around the Purkinje cell (PC) population [4, 6, 11, 12, 16, 25, 28, 31, 33–35, 39, 48], distinguishing ET from matched control brains. These changes are observed in the PC dendritic arbor and PC axonal compartment as well as the connections between PCs and neighboring neuronal populations; some studies have also detected PC loss [4, 11, 16, 25, 28, 31, 33–35, 48]. The discovery of ET-related pathology has generated great interest in the field, but it has also generated debate and raised additional questions [13]. Several of the observable pathological changes have also been noted in other neurodegenerative disorders of the cerebellum such as spinocerebellar ataxias (SCAs) [2, 15, 20, 21, 23, 34, 42, 43, 45] and multiple system atrophy (MSA) [1, 34, 47]. However, the degree to which each of these changes occurs in SCA and MSA, and the relative presence or absence of changes with respect to one another, has not been formally studied. Furthermore, the cerebellum, as part of a larger tremor loop, has been postulated to be involved in other tremor disorders such as

Parkinson's disease [10, 14, 37, 41] and dystonia [5, 7, 17, 18, 44], but whether the pattern of cerebellar pathologic changes seen in ET occurs in these diseases is unknown.

At present, an overriding question in the ET field is whether the morphological changes in the ET cerebellum are distinctive to ET or merely a generic feature of neurodegenerative diseases that involve the cerebellum. These changes have not been contextualized within a broader degenerative disease spectrum, thereby limiting their interpretability. To address this question, we performed a comparative analysis of quantitative morphologic changes in cerebellar cortex in a postmortem study of 156 brains (50 ET, 23 SCA, 15 MSA, 29 Parkinson's disease, 14 dystonia, 25 controls), with metrics reflecting alterations in the cell body, dendritic and axonal compartments of PCs, basket neuron axons and afferent climbing fiber synaptic inputs. We hypothesized that there might be a particular profile of cerebellar changes (i.e., a disease signature) in ET and this is likely distinct from those of other neurodegenerative disorders that involve the cerebellum. We use the term "*patholog-omic profile*" to try to encapsulate this notion of a distinct profile of pathological changes.

Materials and methods

Brain repository, study subjects, and clinical assessment

ET brains were from the Essential Tremor Centralized Brain Repository (ETCBR), a longstanding, joint collaboration between investigators at Yale and Columbia Universities [33]. The ETCBR serves ET cases in the United States. ET diagnoses were carefully assigned by a senior movement disorder neurologist (E.D.L.) utilizing three sequential methods [4]. Briefly, the clinical diagnosis of ET was initially assigned by treating neurologists, and secondly, confirmed by E.D.L. using questionnaires, review of medical records and review of Archimedes spirals. Third, a detailed, videotaped, neurological examination was performed and action tremor was rated and a total tremor score assigned [range = 0–36 (maximum)]. Combined with the questionnaire data, the final diagnosis of each ET case was re-examined, using previously published diagnostic criteria, which have been shown to be both reliable and valid [4]. None of the ET cases had a history of traumatic brain injury, exposure to medications with associated cerebellar toxicity (e.g., chemotherapeutic agents), or heavy ethanol use, as defined [4, 19]. Every 6 months, a follow-up semi-structured telephone evaluation was performed on ET cases and hand-drawn spirals were collected.

Twenty-two control brains were from the New York Brain Bank. These individuals were prospectively followed at the Alzheimer's Disease Research Center or the Washington Heights Inwood Columbia Aging Project at Columbia University. During serial neurological examinations, these individuals were clinically free of ET and other neurodegenerative disorders, including Alzheimer's disease, Parkinson's disease, or progressive supranuclear palsy [33]. Three control brains were obtained from the National Institutes of Health NeuroBioBank (University of Miami, Miami, FL, USA).

We were able to obtain 23 SCA brains (ten SCA1, five SCA2, six SCA 3, two SCA6) from multiple brain repositories: 16 from a hereditary ataxia specimen repository maintained by a coauthor (A.H.K.) at the Veterans Affairs Medical Center in Albany, New York, 6 from the

National Institutes of Health NeuroBioBank (University of Maryland, Baltimore, MD, USA), and 1 from the New York Brain Bank. We grouped the SCA1, SCA2 and SCA6 brains together (i.e., "SCA1/2/6") as these disorders are characterized by marked PC loss; in contrast, SCA3 is not characterized by marked PC loss. Tissue from 29 Parkinson's disease brains was obtained from the New York Brain Bank. We also obtained 15 MSA brains and 14 dystonia brains from several sources (see Acknowledgements). All study subjects signed informed consent forms approved by the respective university or institutional ethics boards.

One-hundred-fifty-six postmortem brains were analyzed. Subject selection was guided by available tissue. We identified 50 ET cases from the New York Brain Bank and selected 25 controls to achieve a 2:1 ratio, selecting older controls whose ages most closely approximated those of the ET cases. ET cases were further selected to lack widespread marked hypoxic-ischemic damage, concurrent Alzheimer'stype changes that would meet criteria for high likelihood of Alzheimer's disease, or evidence of other neurodegenerative disease pathology (e.g., progressive supranuclear palsy, corticobasal degeneration, Lewy bodies, traumatic encephalopathy). We performed power analyses utilizing data from our previous publications on dendritic swellings in ET cases and controls (1.50 ± 1.79 vs. 0.05 ± 0.23 per section) [48], torpedoes in ET cases and controls (15.2 ± 12.1 vs. 2.9 ± 2.1 per section) [34], and PC counts in ET cases and controls (3.6 ± 0.5 cells/mm vs. 4.9 ± 0.7 cells/mm) [11]. Assuming alpha = 0.05, and two-sided Student's t tests, a sample of 50 ET cases and 25 controls would provide > 97% power to detect a change in each metric in ET cases of similar magnitude to that demonstrated previously. Cerebellar pathology in the SCA cases was expected to be double that of ET cases [33, 34]. We utilized all available 23 SCA brains, with a minimum number of five brain samples for each of the two SCA groups (i.e., for these analyses, 6 SCA3 and 17 SCA1/2/6), and this provided > 95% power (alpha = 0.05; two-tailed) to detect differences between each SCA group and controls. We aimed to set the number of Parkinson's disease brain tissue approximately equal to controls, and were able to obtain 29, preferentially selecting the oldest cases first so as to achieve an age distribution that approached that of our controls and ET cases. Utilizing data from our previous publication on torpedoes in Parkinson's disease cases and controls (6.1 ± 6.3 vs. 2.0 ± 1.6 per section) [31], our Parkinson's disease and control sample provided > 90% power to detect a change in this metric in Parkinson's disease cases of similar magnitude to that demonstrated previously. We were able to obtain 14 dystonia brains. There are few studies of pathological features of dystonia, although the major study found a significant reduction in PC counts ($p < 0.05$) with only 6 cervical dystonia and 13 controls [40]. Similarly, an earlier study reporting data on torpedo and PC counts detected significant differences between the groups ($p < 0.001$) with only 8 MSA cases and 27 controls [34]; in the current study, we had 15 MSA brains. In summary, our study was adequately powered to detect cerebellar pathology across different diagnoses.

Tissue processing and initial examination

Brains from the New York Brain Bank had a complete neuropathological assessment with standardized measurements of brain weight (grams) and postmortem interval (hours between death and placement of brain in a cold room or upon ice) [4]. Whenever possible, 17 standardized blocks were harvested from each brain and processed, and 7 μm thick paraffin

sections were stained with Luxol fast blue/hematoxylin and eosin (LH&E) [32]. In addition, selected sections were stained by the Bielschowsky method, and with mouse monoclonal antibodies to alpha-synuclein (clone KM51, Novocastra), phosphorylated tau (clone AT8, Research Diagnostics, Flanders, NJ, USA) and beta-amyloid (clone 6F/3D, Dako, Carpinteria, CA, USA) [32]. All tissues were examined microscopically by a senior neuropathologist (J.P.G.V.) blinded to clinical information [32]. Brains had Braak and Braak Alzheimer's disease staging for neurofibrillary tangles, and Consortium to Establish a Registry for Alzheimer's disease (CERAD) ratings for neuritic plaques [8, 9, 26, 38]. Thal stage was also assigned [46]. Cerebellar tissues received from other brain repositories were from the same standard region as harvested at the New York Brain Bank. In most instances, brain weights (grams) were available, and in some instances, data were also available on postmortem interval, Braak Alzheimer's disease staging and CERAD staging. All cerebellar specimens in this study were stained for beta-amyloid to determine whether amyloid plaques were present.

Quantification of PCs, torpedoes and related cerebellar pathology

A standard $3 \times 20 \times 25$-mm formalin-fixed tissue block from each brain was obtained from a parasagittal slice located 1–1.5 cm from the cerebellar midline and containing anterior and posterior quadrangulate lobules and the underlying dentate nucleus. This block was used to quantify 37 metrics within the following eight broad categories of pathological change: (1) PC loss, (2) heterotopic PCs, (3) PC dendritic changes, (4) PC axonal changes (torpedoes), (5) PC axonal changes (other than torpedoes, e.g., recurrent collaterals, thickened axons), (6) PC axonal changes (torpedo-associated), (7) basket cell axonal hypertrophy, (8) climbing fiber-PC synaptic changes. Within each category, there were one or more metrics, totaling to 37 metrics in eight categories (Table 1, Fig. 1, Supplemental Fig. 1). Several of the metrics were normalized by dividing by the PC layer length to account for variations in amount of cerebellar cortex in the tissue block and/or microscopic field imaged, and were expressed as mm^{-1}. Other metrics were divided by the number of PCs, to account for PC loss, which may affect the ability to detect the pathologic change. More specifically, we created nine metrics that adjusted for the number of PCs, which are parallel to nine metrics created that do not adjust for number of PCs. The rationale to adjust these metrics for number of PCs is the concern that in the setting of severe PC loss, the value for the metric would be artificially low. For example, it stands to reason that in the setting of PC loss, that both the counts for displaced PCs (i.e., heterotopic PCs) and the counts for normally placed PC would be low. Morphologic changes were identified by a variety of methods, including histologic stains (LH&E, Bielschowsky), immunostain for calbindinD_{28k} on 100 μm thick vibrotome sections [4], dual immunostain for calbindin$_{28k}$ and glutamic acid decarboxylase (GAD) [27], and immunostain for vesicular glutamate transporter type 2 (VGlut2) [22, 28] (Table 1). The composite of multiple metrics provided a complete view of pathological changes, which one metric alone was unable to provide. Each category of pathological change is now described in detail.

PC cell loss

PC loss has been detected in some studies of ET [3, 11, 32]. The metrics in this category include three measures of PC linear density, which differ with respect to the structures

counted (e.g., PC cell bodies or PC nucleoli) and staining method (LH&E or calbindinD$_{28k}$ immunostain). Dual immunohistochemical staining for calbindinD$_{28k}$ and GAD was also performed and "empty baskets" were identified as the plexus of basket cell axons around the PC soma without a detectable PC body; the percentage of empty baskets has been shown to be elevated in ET and provides an indirect measure of PC loss [27].

Heterotopic PCs

Heterotopic PCs are those whose cell body is misplaced in the molecular layer; such heterotopic misplacement is more prevalent in ET than control brains, and may reflect an untethering of remaining PCs in the setting of PC loss [33]. The metrics in this category include four measures of the number of heterotopic PCs, which differ with respect to the staining method (LH&E or c albindinD$_{28k}$ immunostain) and whether they were normalized to PC layer length or to the number of PCs.

PC dendritic changes

Focal swellings of PC dendritic processes, defined as rounded-to-ovoid masses in the molecular layer that are associated with PC dendrites [48] were quantified with six metrics. The six metrics differ with respect to the staining method (LH&E, Bielschowsky, or calbindinD$_{28k}$ immunostain) and whether they were normalized to PC layer length or to the number of PCs.

PC axonal changes (torpedoes)

Common among the axonal changes in ET are torpedoes, which are round or ovoid swellings of the proximal portion of the PC axon; these are easy to visualize using numerous methods. In this category are seven metrics that differ with respect to the staining method used (in order of increasing sensitivity: LH&E, Bielschowsky, calbindinD$_{28k}$ immunostain), whether they were normalized to PC layer length or to the number of PCs, and whether axons with single torpedoes or axons with multiple torpedoes were counted.

PC axonal changes other than torpedoes

A variety of additional changes in PC axonal anatomy have been described in ET, including PC axonal recurrent collaterals (at least a 90° turn back towards the PC layer from their initial trajectory), PC thickened axonal profiles (axons at least double the width of other apparently normal axons), and PC axonal branching (any axon with at least one branch point) [4]. Other metrics were: the PC plexus percentage (the percent of the length of the PC layer covered by a visible recurrent collateral plexus) [4] and PC puncta (the number of PCs with several dark puncta along the PC soma and proximal dendrites; while the etiology of this change is not fully established, it is thought to represent the synapses of PC recurrent collaterals or aggregates of degenerating PC cytoplasm). PC terminal axonal sprouting (the presence of a frayed terminal axonal region, often with a kinky appearance) was rated using a 0–3 scale: 0 (no visible sprouting); 0.5 (up to two instances of simple sprouting); 1 (at least three instances of simple sprouting or up to 2 instances of complex sprouting); 1.5 (at least three instances of simple sprouting and up to 2 instances of complex sprouting); 2 (widespread simple sprouting and/or at least 3 instances of complex sprouting); 2.5

(widespread complex sprouting); 3 (most axons exhibiting complex sprouting) (Supplemental Fig. 1). In this category, the seven metrics all are based on calbindinD$_{28k}$ immunostains of 100 μm thick cerebellar sections.

PC axonal changes (torpedo-associated)

In ET, PCs with torpedoes are more likely to have additional axonal changes (e.g., thickened profiles, recurrent collaterals, branching) than PCs without torpedoes [4]. The six metrics in this group assess axonal changes in PCs with torpedoes; the metrics are normalized either to the number of torpedoes (%) or the PC layer length (per mm). These metrics all are based in calbindinD$_{28k}$ immunostains of 100 μm thick cerebellar sections.

Basket cell axonal hypertrophy

This category includes a single metric—a semi-quantitative rating of the density of the basket cell axonal plexus surrounding PC bodies in Bielschowsky stain, with a scale of 0–3 [16]. This density is increased in ET, and likely reflects a secondary response to PC loss [16].

Climbing fiber-PC synaptic changes

This category includes two metrics assessing the distribution of climbing fiber-PC synapses on PC dendrites. One is a measure of the density of these synapses and the other is a measure of the redistribution of these synapses to the parallel fiber synaptic territory in the outer 20% of the molecular layer [28].

Statistical analyses

Demographic and primary pathological features across diagnostic categories —Clinical and pathological features of each diagnostic group were compared (Table 2). As discussed above, we grouped SCA1, 2 and 6 brains together (i.e., "SCA1/2/6"). Categorical or ordinal variables were compared using Chi-square tests. For continuous variables, we tested for normality using the Kolmogorov–Smirnov test. Continuous variables were compared using Student's *t* tests or, if not normally distributed, a non-parametric test (i.e., Mann–Whitney).

Correlation between demographic and primary pathological features and quantitative morphologic metrics—For each of the eight categories of pathological features, we selected one metric that had high sensitivity (e.g., the metric was characterized by higher rather than lower values when compared with controls) and that provided high discrimination between values in our highest vs. lowest groups (i.e., SCA1/2/6 vs. controls). For PC counts, the inverse (i.e., PC^{-1}) was used so that higher values were more pathologic. For each of these "core metrics", values were normalized to 1 (i.e., the mean of each of the eight metrics was determined as well as the value that the mean would need to be multiplied by to be 1.0. For example, if the mean = 0.5, then that value would be 2.0. Then each data point in each brain was multiplied by this value. This operation was performed separately for each of the eight metrics).These eight core metrics, all median values unless otherwise specified, were: (1) the inverse of the PC body count per mm (LH&E stain), (2) heterotopic

PCs per PC (LH&E stain), (3) PC dendritic swellings per mm (Bielschowsky stain), (4) torpedoes per mm (calbindin$_{D28k}$ immunostain), (5) thickened Purkinje cell axons per mm (calbindin$_{D28k}$ immunostain), (6) torpedoes with recurrent collaterals per mm (calbindin$_{D28k}$ immunostain), (7) rating of basket cell axonal hypertrophy (Bielschowsky stain, mean value), (8) climbing fiber-Purkinje cell synapses in outer 20% of molecular layer (VGlut2 immunostain).

We then assessed whether the eight core metrics were correlated with age, gender, brain weight, Braak Alzheimer's disease staging, CERAD and postmortem interval. These analyses, using Spearman's rho, used our core sample of brains with similar age distribution (controls, dystonia, Parkinson's disease) to avoid detecting correlations with age that were spurious (i.e., due to age differences across diagnoses). Given the large number of comparisons ($n = 48$), using a Bonferroni correction we set the significant p value at < 0.001 (i.e., 0.05/48).

Several additional analyses were performed. First, in ET cases, we correlated each of the 37 metrics with total tremor score and with disease duration, using Spearman's rho. To further assess how each of the metrics could have been influenced by postmortem factors such as postmortem delay in our ET cases, we also correlated each of the 37 metrics with postmortem interval.

Principal component analysis (identifying underlying dimensions)—Given the large number of metrics ($n = 37$), a principal component analysis was first performed to identify underlying unifying dimensions (i.e., groupings of metrics) and to obtain a broad overview of the distribution of the data points. This analysis used z scored raw data for each metric across all diagnostic categories. For this analysis, we used the *PCA* function in Python's *scikit-learn* package to compute the principal components of the z scored data. We used Pearson's correlation coefficients to determine the correlation between each metric and each principal component.

Quantifying change in each metric in each diagnosis—We next quantified change in each metric across diagnoses, using controls as our reference group. To compute an average fold-change effect size for each metric in each diagnosis, we first calculated the average value of the control samples for each metric and the average value of each diagnosis' samples for each metric. Then, for each metric and diagnosis, we computed the log$_2$-ratio of these two average values. We evaluated the statistical significance of these changes relative to controls using the Mann–Whitney test and corrected the resulting p values for false discovery using the Benjamini–Hochberg method. As there were differences in age between several diagnoses and controls, we adjusted for the effects of age using a series of multiple linear regression models. Therefore, for each diagnosis, there were 37 models, with the dependent variable = metric data and independent variables = diagnosis (disease vs. control) and age. We then compared the effect sizes in these adjusted models with those in our unadjusted analyses, using Spearman's rho.

Determining whether there is a core signature of cerebellar degeneration—To formally determine whether there was a robust co-varying core signature of cerebellar

degeneration, the correlation between all pairwise combinations of metrics was computed and the correlation coefficients were hierarchically clustered.

Examining patterns of change across diagnoses—We also generated three violin plots: (1) a "Severity Score" containing the core set of 20 highly correlated metrics, (2) a "PC Loss Score" [inverse PC body/mm, inverse PC nucleolus/mm, percentage empty baskets], and (3) climbing fibers in the outer 20% of the molecular layer.

Last, to further delineate the disease pattern in controls and ET vs. primary disorders of cerebellar degeneration (SCAs), we compared data from our eight core metrics to show their deviation from the norm in a skyline plot.

Developing a neuropathological scoring system—We developed a cumulative score derived from the morphologically most evident and biologically most relevant metrics. This comprised ten metrics, as indicated by an asterisk in Table 3 (although the inverse of LH&E PC/mm was used). For ET, controls and each of the remaining diagnoses, we reported the median, mean, 25th quartile and 75th quartile score for this "ET neuropathological score".

Results

Demographic and primary pathological features across diagnostic categories

We examined pathological changes (Table 1) in the cerebellum in controls vs. a spectrum of neurologic disorders including ET, dystonia, Parkinson's disease, SCA3, SCA1/2/6 and MSA. Several of the groups differed with respect to age, Braak score, CERAD score and postmortem interval (Table 2). Some of these differences were expected given the natural history of these disorders, with younger ages of onset in SCAs and MSA than in ET or Parkinson's disease.

Correlation between demographic and primary pathological features and quantitative morphologic metrics

We generated data on 37 quantitative morphologic metrics obtained through histologic and immunohistochemical stains to detect changes in PCs (soma, dendrites, axons), basket neuron axons and climbing fiber synapses. The metrics were grouped into 8 broad categories (see "Materials and methods", Table 1, Fig. 1). We selected one metric from each of the eight categories (see "Statistical analyses" in methods) and assessed whether these eight core metrics were correlated with age, gender, brain weight, Braak Alzheimer's disease staging, CERAD and postmortem interval. These analyses, using Spearman's rho, utilized our core sample of brains that had a similar age distribution (controls, dystonia, Parkinson's disease). Given the large number of comparisons ($n = 48$), we set the significant p value at < 0.001. None of the correlations reached significance (i.e., all p 0.001), indicating that differences between diagnostic groups in these variables (e.g., age, gender) were not likely to account for differences in cerebellar pathology between diagnostic groups.

Several additional analyses were performed. First, in ET cases, we correlated each of the 37 metrics with total tremor score and with disease duration, using Spearman's rho. Two of the torpedo counts were correlated with disease duration, but otherwise the correlations were not

significant (Supplemental Table 2). To further assess how each of the metrics could have been influenced by postmortem factors such as postmortem delay, in our ET cases we also correlated each of the 37 metrics with postmortem interval. In these analyses, none of the metrics was correlated with postmortem interval, with r values ranging from 0.01 to 0.25 and p values ranging from − 0.99 (data not shown).

Principal component analysis (identifying underlying dimensions)

Given the large number of metrics and data generated (37 metrics in 156 brains = 5772 data items), a principal component analysis of the *z* scored raw data was first performed to identify underlying unifying dimensions (i.e., groupings of metrics) and to obtain a broad overview of the distribution of the data points. When analyzed across all diagnostic categories, the two major axes of variation in the data segregated individual patients into distinct groupings (Fig. 2a). To a large extent, the first axis of variation (principal component 1) separated MSA and SCA1/2/6 from the remaining diagnoses, with the data points in MSA and SCA1/2/6 distinctly situated to the right of the main cluster. Metrics that were highly correlated to principal component 1 (i.e., they were major influencers of principal component 1) were torpedo counts (green bars), several torpedo-associated changes in PC axons (dark blue bars) and PC dendritic swellings (yellow bars) (Fig. 2b). These metrics had higher values in MSA and SCA1/2/6. In contrast, metrics that were anti-correlated with principal component 1 reflect less PC loss (purple bars) and better-preserved climbing fiber synapses (light blue bars). The second axis of variation (principal component 2) mainly separated MSA from SCA1/2/6, with most data points for SCA1/2/6 located below those of MSA (Fig. 2a). Metrics that were highly correlated to principal component 2 (i.e., they were major influencers of principal component 2) were most calbindin PC axonal changes (orange bars) except for PC puncta, torpedo-associated changes in PC axons (dark blue bars), torpedo counts (green bars) and better-preserved PC counts (purple bars) (Fig. 2c). Principal component 2 anti-correlated values included greater percentage of empty baskets (purple bar, i.e., more PC loss), dendritic swellings (yellow bars), and calbindin PC puncta (orange bars). Thus, this initial analysis predominantly highlights distinct differences in morphologic changes between SCA1/2/6 and MSA vs. other disease categories and between SCA1/2/6 and MSA.

While controls, ET, Parkinson's disease and dystonia form a dense cluster (Fig. 2a), there is not complete overlap, and variable segregation is apparent predominantly along the axis of principal component 1 when MSA and all SCAs are excluded from the analysis (Fig. 2d). All but one control sample (black dots) has a principal component 1 value < − 0.50, and the median of all controls centers at principal component 1 = − 2.37. Compared to controls, dystonia (light blue dots, median principal component 1 = − 0.97) and Parkinson's disease (green dots, median principal component 1 = − 0.78) patients are shifted to the right, and ET patients (red dots) are even further shifted to the right (median principal component 1 = 1.53). Metrics correlating strongly with principal component 1 include torpedo counts (green bars), calbindin torpedo-associated changes with thickened-, recurrent-, and branching-PC axons (dark blue bars), dendritic swellings (yellow bars) and calbindin thickened PC axons (orange bar) (Fig. 2e). These metrics had higher values in ET than controls. There is also a notably stronger positive correlation for VGlut2 outer 20% and basket cell rating, consistent

with their enrichment in the ET cerebellum vs. controls. Anti-correlated metrics were preserved PC counts (purple bars) and climbing fiber synaptic density (light blue bar).

We also compared the principal component data for ET and all SCAs, as disorders whose primary identifiable pathology is most evident in the cerebellum, vs. controls (Fig. 2f). The distribution of data for ET (red dots) and SCA3 (orange dots) are shifted to the right vs. controls (black dots) along the principal component 1 x-axis, with median values at -2.45 (controls), -1.05 (ET) and -0.47 (SCA3). Notably, there is significant overlap in data points for SCA3 and many ET cases. SCA1/2/6 patients (blue dots) are shifted to a much greater extent along both principal component 1 (median = 6.16) and principal component 2 axes. The distribution of SCA1/2/6 cases along the principal component 1 x-axis reflects varying disease severities that correlated with severity of PC loss, centered at 4.20 for SCA1, 6.98 for SCA2 and 9.78 for SCA6.

In summary, these analyses showed that these diagnoses were not uniform with respect to cerebellar pathology, with the greatest (though not identical) changes observed in MSA and SCA and lesser changes in the other groups (Fig. 2a–e). In terms of primary disorders of cerebellar degeneration, the changes lay along a spectrum, with those observed in ET and SCA3 being the mildest and those in SCA1/2/6 being the most severe relative to controls (Fig. 2f). As a whole, each of these disorders occupies a distinctive space along a spectrum of cerebellar of degeneration.

Quantifying change in each metric in each diagnosis

We next quantified the change in each metric across diagnoses, using controls as our reference group (Fig. 3a). Metrics (rows) and diagnoses (columns) are shown. Each cell in the heatmap is the average $\log_2$-fold-change (disease vs. control) for each metric. Dark purple cells indicate that there is a high mean value for the metric relative to controls and green indicates the opposite. Elements labeled with an asterisk indicate that the difference from controls is statistically significant, with false discovery rate < 0.01. Several observations may be made.

First, when compared to controls, dystonia and Parkinson's disease differed significantly in only 2/37 metrics (see two asterisks). In contrast, the number of differing metrics was 21 for ET, 8 for SCA3, 19 for MSA, and 26 for SCA1/2/6 (Fig. 3a).

Second, in terms of categories of pathological change, dystonia and Parkinson's disease significantly differed from controls in 2/8 categories; SCA3 differed in only 3/8 categories (Fig. 3a, Supplemental Table 1). ET and SCA1/2/6 each significantly differed from controls in 7/8 categories, and MSA from controls in 6/8 categories (Fig. 3a, Supplemental Table 1).

Third, in 17 metrics across 6 categories (i.e., PC loss, heterotopic PCs, PC dendritic changes, PC axonal changes [torpedoes], PC axonal changes [other than torpedoes], and PC axonal changes [torpedo-associated]), neither dystonia nor Parkinson's disease differed from controls, yet there was a spectrum of change, with ET generally at the low end and SCA1/2/6 or MSA at the high end of severity (Fig. 3a, Table 3).

Fourth, for three metrics, including the percentage climbing fibers in the outer 20% of the molecular layer (VGlut2) and two metrics involving PC puncta (calbindinD$_{28k}$), the pattern observed for ET was not merely on the cerebellar degeneration spectrum. The mean percentage of climbing fibers in the outer 20% of the molecular layer (VGlut2) was distinctly increased in ET compared to controls, whereas in SCA1/2/6 and MSA there was a decrease compared with controls (Fig. 3a, c). The density of PC puncta (calbindin) and PC puncta per PC (calbindin) (Fig. 1R, R′) was only significantly increased in SCA1/2/6, and involving a larger percentage of PCs when seen in a sample. In control, ET or MSA samples, these structures were rare.

As there were differences in age between several diagnoses and controls, we adjusted for the effects of age using a series of multiple linear regression models. We then compared the effect sizes in these adjusted models with those in our unadjusted analyses, using Spearman's rho. The effect sizes (i.e., fold-difference in each metric between each disease and control) were strikingly similar as were the direction of these differences, indicating that observed differences in the unadjusted analyses were nearly universally conserved in the age-adjusted analyses (Supplemental Fig. 2).

Finally, in our primary analyses we grouped SCA1/2/6 together. For a secondary analysis, we examined the spectrum of changes in each of the 37 metrics across these SCA subtypes (Supplemental Fig. 3). Overall, the three SCA subtypes were broadly similar in the direction of fold-change vs. controls (i.e., purple and green colors indicates increased vs. decreased, respectively) when samples were either grouped (Fig. 3a) or separated out (Supplemental Fig. 3). There were some differences in terms of the extent of fold-change between these SCAs, as demonstrated by the color saturation, indicating that these SCA subtypes, though broadly similar, are not identical.

Determining whether there is a core signature of cerebellar degeneration

To formally determine whether there was a robust co-varying core signature of cerebellar degeneration, the correlation between all pairwise combinations of observables was computed and the correlation coefficients were hierarchically clustered (Fig. 3b). A large red block of observables (20 metrics) was all strongly positively correlated with each other and represent a core, common phenotypic signature mainly related to torpedoes, other axonal changes and dendritic swellings (red asterisks). Two other metrics (CB % torpedoes with recurrent axon, calbindin-GAD % empty baskets) are a secondary node of predominantly positively correlated metrics, although with more variability (orange asterisks). Other metrics were anti-correlated (Fig. 3b, blue squares and asterisks), consistent with their inverse relationship to torpedo pathology (e.g., PC count metrics) or a more common tendency to lose climbing fiber synapses in cerebellar disease [24]. In sum, these co-varying morphologic metrics defined "Key Drivers" of cerebellar pathology, which correlated with many of the statistically significant differences across disease categories (Fig. 3a, red, orange and blue asterisks).

Examining patterns of change across diagnoses

Next, we computed scores for each patient as a fold-change relative to control averaged over selected observables and plotted on a $\log_2$-transformed scale (Fig. 3c), including (1) a "Severity Score" containing the core set of 20 highly correlated observables (Fig. 3b, red asterisks), (2) a "PC Loss Score" [inverse PC body/mm, inverse PC nucleolus/ mm, percentage empty baskets], and (3) climbing fibers in the outer 20% of the molecular layer. The "Severity Score" differed significantly across all diagnoses, with a gradual increase from dystonia to Parkinson's disease to ET, was intermediate for SCA3, and high for MSA and SCA1/2/6. The PC loss score is higher in ET than in control, dystonia, Parkinson's disease or SCA3, is widely variable in MSA, and highest in SCA1/2/6. Along with the climbing fiber outer 20% score, which shows a distinct increase in ET vs. all other diagnoses, these data demonstrate that ET had both common and distinctive combinations of morphologic patterns across a spectrum of cerebellar degeneration.

Several of these disease patterns across diagnostic categories are observed in c albindinD_{28k} immunostained cerebellar sections (Fig. 4). Changes in PC axonal shape (e.g., torpedoes, thickened axons) and connectivity (e.g., recurrent collaterals, axonal branching) and PC body loss were less apparent in dystonia and Parkinson's (Fig. 4b, c) than ET (Fig. 4d, e), and heterotopias and dendrite swellings were more frequent in ET. Despite the relative preservation of PCs in SCA3, PC axonal changes and occasional heterotopic PCs are seen (Fig. 4f), along with dendrite swellings (not shown). Both SCA1/2/6 and MSA showed a wide range of PC loss, along with marked increases in PC axonal changes (Fig. 4g–l). A more variable PC loss in MSA often resulted in quite abundant torpedo formation, with some PC axons extending into better-preserved white matter (Fig. 4j), whereas areas of more severe white matter degeneration showed many torpedoes associated with prominent recurrent axons (Fig. 4k), indicating a greater disconnection of PCs from their target cerebellar nuclei, perhaps replaced by reorganization of intracortical cerebellar circuitry.

Last, to further delineate the disease pattern in controls and ET vs. primary disorders of cerebellar degeneration (SCAs), we compared data from our eight core metrics to show their deviation from the norm in a skyline plot (Fig. 5). Notably, controls had values that were lowest and SCA1/2/6 the highest, whereas ET and SCA3 were intermediate. Yet the patterns of pathological changes observed in ET, SCA3, and SCA1/2/6 differed from one another, with the relative heights of the bars to one another varying both within and across diagnostic categories. Thus, it is apparent that ET, SCA3 and SCA1/2/6 differed with respect to the relative expression (i.e., signature) of the degenerative features. For instance, it is well-known that PC loss is not a feature of SCA3, which can be seen by a similar height of the purple bar to that in controls; nonetheless, there are still increased changes related to torpedoes (dark blue, green and orange bars) in SCA3 vs. that in controls and ET, and dendrite swellings (yellow bar) are similarly increased in ET and SCA3 vs. controls. In contrast, in ET, the redistribution of climbing fiber synapses to the outer 20% of the PC arbor is highest (light blue bars), whereas climbing fiber synapses are markedly destroyed in SCA1/2/6 and also not present in the parallel fiber domain in SCA3. PC dendritic swellings and heterotopias are the most prominent in SCA1/2/6 in comparison to all other diagnoses.

Developing a neuropathological scoring system

We developed a cumulative score derived from the morphologically most evident and biologically most relevant metrics, representing each category of pathological change. This comprised 10 metrics, selected on the basis of their strength in differentiating disease diagnoses in the principal component analysis and control-disease fold-change analyses (Figs. 2, 3a). Next to each of the 10 metrics is an asterisk (Table 3; the inverse of LH&E PC/mm was used). For ET, controls and each of the remaining diagnoses, we reported the median, mean, 25th quartile and 75th quartile score for this ET neuropathological score (Supplemental Table 3). The median score for ET was slightly higher than that for SCA3, approximately double that of PD, triple that of dystonia and 20-times higher than that of controls. It was a third that of MSA and SCA1/2/6 (Supplemental Table 3). Furthermore, there was diagnostic separation between ETs and controls, with the score for the lower 25% quartile of ET cases (0.391) exceeding the upper 75% quartile of controls (0.283). Last, there was a significant correlation between the ET scores and disease duration (Spearman rho = 0.29, $p = 0.044$).

Discussion

During the past decade, numerous morphological changes have been identified in the ET cerebellum. However, these changes have not been contextualized within a broader degenerative disease spectrum, thereby limiting their interpretability. Thus, a central question in the ET field is whether the morphological changes observed in the ET cerebellum are distinctive to ET or merely a generic feature of most neurodegenerative diseases of the cerebellum. To address this issue, we used an "omics" approach to gain a "systemwide" understanding of these pathological changes. Here, we identified metrics that characterized stereotypic cellular responses in cerebellar disease as well as patterns of changes that differentiate ET and other disorders in the spectrum of cerebellar degenerative diseases.

In these analyses, which used more than 5000 data items, we make several core observations. First, although changes were observed in the cerebellum of dystonia and Parkinson's disease, they were not nearly of the number/magnitude observed in disorders whose primary identifiable pathology is most evident in the cerebellum (i.e., ET, SCA3, SCA1/2/6 and MSA to some extent) (Figs. 2a, d, 3a). Second, within the latter grouping, there was a marked spectrum of change, with ET generally at the low end and SCA1/2/6 or MSA at the high end of severity (Figs. 2f, 3a, c). In this sense, the changes observed in ET fall on the mild end of what is observed in cerebellar degenerations. In large part, these comprised differences of *degree* rather than *kind*, with co-varying metrics that had a positive or negative fold-change relative to controls, likely reflecting a stereotypic repertoire of cellular reactions that characterize cerebellar degeneration. Third, features distinctive to specific disorders were also identified, including a unique redistribution of climbing fiber synapses to the outer PC dendritic arbor in ET and aggregation of c albindinD$_{28k}$-positive puncta around the PC soma most prominently in SCA1/2/6 (Fig. 3a). Each of these disorders had a different signature with respect to cerebellar degeneration, as evidenced by our metric "scores" that combine categories of morphologic features (Fig. 3c) and a skyline plot (Fig.

5), which showed that different patterns emerged for ET, SCA3, and SCA1/2/6, indicating that these disorders of cerebellar degeneration do not form a homogeneous entity. In this sense, there were differences not only of *degree*, but also of *kind*.

The pathological changes in the PC and neighboring neuronal populations are not occurring in isolation with respect to one another; indeed, they operate as part of a system rather than in seclusion, as suggested by the array of morphologic changes that formed core "Key Drivers" of cerebellar pathology (Fig. 3a, b). Some of the changes are primary whereas others are likely to be responsive, secondary, and reparative. Among these disorders, the mechanism of cerebellar cortical degeneration varies, highlighted by the morphologic metrics we analyzed. In SCA3, for example, there is relative preservation of PCs. As a result, secondary changes that are observed in ET, such as basket cell axonal hypertrophy and heterotopic un-anchoring of PCs in the setting of PC loss, are less apparent in SCA3. While the brunt of cerebellar degeneration affects the dentate nucleus in SCA3 [23], we still detected significantly increased PC dendrite swellings, torpedoes and decreased climbing fiber synaptic density, to our knowledge quantified here for the first time. These cerebellar cortical changes in SCA3 may predominantly reflect a dyingback-type PC degeneration due to loss of PC terminals in the dentate and climbing fiber regression secondary to mild PC dendrite changes and/or brainstem degeneration that may include mild neuronal loss in the inferior olive [43]. With regressive changes in the dendritic arbor in ET likely more common than total loss of the PC [35], the redistribution of climbing fiber synapses to the outer 20% of the PC arbor is highest and a distinctive feature of ET. In contrast, in more severe forms of cerebellar degeneration, with more PC loss (e.g., in SCA1/2/6), this morphological change is less often observed. Thus, it is plausible that the changes observed in ET are those of a milder, slowly progressive disorder of PC homeostasis, characterized by changes in PC function and anatomy with accompanying dendritic and axonal changes, some degree of PC loss, and the advent of secondary changes (basket cell axonal hypertrophy, redistribution of climbing fiber-PC synapses, untethering of PCs with resultant heterotopic displacement).

We also developed an "ET neuropathological score", which in the future might be of value for diagnostic purposes, although further studies are needed to test and validate these as possible criteria. In the current dataset, the value for ET was slightly higher than that for SCA3, approximately double that of PD, triple that of dystonia and 20-times higher than that of controls. It was a third that of MSA and SCA1/2/6 (Supplemental Table 3). There was some separation between ET and control scores, and the ET scores showed correlation with disease duration. This score should be viewed as a preliminary construct that is ripe for additional testing.

This study is the first of its kind, where we applied an "omics" approach to study disease-associated morphologic changes in cerebellum. However, our findings should be interpreted within the context of limitations. First, although dealing with more than 150 brains, for some diagnoses, the number of available brains was small. Nonetheless, sample size calculations indicated that the number of brains was sufficient and, indeed, differences were easily detectable for samples with low numbers, such as the SCAs. Second, there was some heterogeneity in the ages of our disease groups. However, in correlational analyses, we showed that age was not correlated with our eight core metrics of pathological change,

indicating that age differences were not likely to account for differences in cerebellar pathology between groups. Third, we restricted our sampling to one region in the cerebellar hemisphere, and it would be of considerable interest in future studies to sample additional cerebellar regions. Fourth, future studies of the dentate nucleus, a site of major pathology in patients with SCA3, and of other pathologies (e.g., glial pathologies including microgliosis), would further add to the neuroanatomical understanding of and ability to derive distinctions between these various diseases of the cerebellum. Strengths of the study include: (1) the large number of brains overall, (2) inclusion of not only ET and control brains, but other neurodegenerative disorders characterized by cerebellar involvement and/or tremor (SCAs, MSA, Parkinson's disease, dystonia), and (3) the ability to compare ET to several forms of SCA, including those in which PC loss is a feature and others in which it is not.

In summary, the degree of cerebellar degeneration in ET aligns it with disorders of cerebellar degeneration, albeit at the milder end of the spectrum. Yet these disorders do not blandly express the same generic pattern of degeneration, with their only distinguishing feature being the degree to which they express that pattern. In fact, there is evidence that a somewhat distinctive signature of degenerative changes marks each of these disorders.

Supplementary Material

Refer to Web version on PubMed Central for supplementary material.

Acknowledgements

References

1. Armstrong RA (2015) Quantitative pathological changes in the cerebellum of multiple system atrophy. Folia Neuropathol 53:193–202. 10.5114/fn.2015.54420 [PubMed: 26443310]

2. Auburger GW (2012) Spinocerebellar ataxia type 2. Handb Clin Neurol 103:423–436. 10.1016/B978-0-444-51892-7.00026-7 [PubMed: 21827904]

3. Axelrad JE, Louis ED, Honig LS, Flores I, Ross GW, Pahwa R et al. (2008) Reduced purkinje cell number in essential tremor: a postmortem study. Arch Neurol 65:101–107. 10.1001/archneurol.2007.8 [PubMed: 18195146]

4. Babij R, Lee M, Cortes E, Vonsattel JP, Faust PL, Louis ED (2013) Purkinje cell axonal anatomy: quantifying morphometric changes in essential tremor versus control brains. Brain 136:3051–3061. 10.1093/brain/awt238 [PubMed: 24030953]

5. Bares M, Filip P (2018) Cerebellum and dystonia: the story continues. Will the patients benefit from new discoveries? Clin Neurophysiol 129:282–283. 10.1016/j.clinph.2017.10.007 [PubMed: 29122444]

6. Beliveau E, Tremblay C, Aubry-Lafontaine E, Paris-Robidas S, Delay C, Robinson C et al. (2015) Accumulation of amyloid-beta in the cerebellar cortex of essential tremor patients. Neurobiol Dis 82:397–408. 10.1016/j.nbd.2015.07.016 [PubMed: 26253607]

7. Bologna M, Berardelli A (2018) The cerebellum and dystonia. Handb Clin Neurol 155:259–272. 10.1016/B978-0-444-64189-2.00017-2 [PubMed: 29891064]

8. Braak H, Alafuzoff I, Arzberger T, Kretzschmar H, Del Tredici K (2006) Staging of Alzheimer disease-associated neurofibrillary pathology using paraffin sections and immunocytochemistry. Acta Neuropathol 112:389–404. 10.1007/s00401-006-0127-z [PubMed: 16906426]

9. Braak H, Braak E (1997) Diagnostic criteria for neuropathologic assessment of Alzheimer's disease. Neurobiol Aging 18:S85–S88 [PubMed: 9330992]

10. Caligiore D, Helmich RC, Hallett M, Moustafa AA, Timmermann L, Toni I et al. (2016) Parkinson's disease as a system-level disorder. NPJ Parkinsons Dis 2:16025 10.1038/npjparkd.2016.25 [PubMed: 28725705]

11. Choe M, Cortes E, Vonsattel JP, Kuo SH, Faust PL, Louis ED (2016) Purkinje cell loss in essential tremor: random sampling quantification and nearest neighbor analysis. Mov Disord 31:393–401. 10.1002/mds.26490 [PubMed: 26861543]

12. Delay C, Tremblay C, Brochu E, Paris-Robidas S, Emond V, Rajput AH et al. (2014) Increased LINGO1 in the cerebellum of essential tremor patients. Mov Disord 29:1637–1647. 10.1002/mds.25819 [PubMed: 24531928]

13. Deuschl G, Elble R (2009) Essential tremor—neurodegenerative or nondegenerative disease towards a working definition of ET. Mov Disord 24:2033–2041. 10.1002/mds.22755 [PubMed: 19750493]

14. Dirkx MF, den Ouden H, Aarts E, Timmer M, Bloem BR, Toni I et al. (2016) The cerebral network of Parkinson's tremor: an effective connectivity fMRI study. J Neurosci 36:5362–5372. 10.1523/JNEUROSCI.3634-15.2016 [PubMed: 27170132]

15. Donato SD, Mariotti C, Taroni F (2012) Spinocerebellar ataxia type 1. Handb Clin Neurol 103:399–421. 10.1016/B978-0-444-51892-7.00025-5 [PubMed: 21827903]

16. Erickson-Davis CR, Faust PL, Vonsattel JP, Gupta S, Honig LS, Louis ED (2010) "Hairy baskets" associated with degenerative Purkinje cell changes in essential tremor. J Neuropathol Exp Neurol 69:262–271. 10.1097/NEN.0b013e3181d1ad04 [PubMed: 20142764]

17. Filip P, Gallea C, Lehericy S, Bertasi E, Popa T, Marecek R et al. (2017) Disruption in cerebellar and basal ganglia networks during a visuospatial task in cervical dystonia. Mov Disord 32:757–768. 10.1002/mds.26930 [PubMed: 28186664]

18. Filip P, Lungu OV, Bares M (2013) Dystonia and the cerebellum: a new field of interest in movement disorders? Clin Neurophysiol 124:1269–1276. 10.1016/j.clinph.2013.01.003 [PubMed: 23422326]

19. Harasymiw JW, Bean P (2001) Identification of heavy drinkers by using the early detection of alcohol consumption score. Alcohol Clin Exp Res 25:228–235 [PubMed: 11236837]

20. Hellenbroich Y, Gierga K, Reusche E, Schwinger E, Deller T, de Vos RA et al. (2006) Spinocerebellar ataxia type 4 (SCA4): initial pathoanatomical study reveals widespread cerebellar and brainstem degeneration. J Neural Transm 113:829–843. 10.1007/s00702-005-0362-9 [PubMed: 16362839]

21. Hoche F, Baliko L, den Dunnen W, Steinecker K, Bartos L, Safrany E et al. (2011) Spinocerebellar ataxia type 2 (SCA2): identification of early brain degeneration in one monozygous twin in the initial disease stage. Cerebellum 10:245–253. 10.1007/s12311-010-0239-9 [PubMed: 21128038]

22. Koeppen AH, Davis AN, Morral JA (2011) The cerebellar component of Friedreich's ataxia. Acta Neuropathol 122:323–330. 10.1007/s00401-011-0844-9 [PubMed: 21638087]

23. Koeppen AH, Ramirez RL, Bjork ST, Bauer P, Feustel PJ (2013) The reciprocal cerebellar circuitry in human hereditary ataxia. Cerebellum 12:493–503. 10.1007/s12311-013-0456-0 [PubMed: 23389921]

24. Kuo SH, Lin CY, Wang J, Sims PA, Pan MK, Liou JY et al. (2017) Climbing fiber-Purkinje cell synaptic pathology in tremor and cerebellar degenerative diseases. Acta Neuropathol 133:121–138. 10.1007/s00401-016-1626-1 [PubMed: 27704282]

25. Kuo SH, Tang G, Louis ED, Ma K, Babji R, Balatbat M et al. (2013) Lingo-1 expression is increased in essential tremor cerebellum and is present in the basket cell pinceau. Acta Neuropathol 125:879–889. 10.1007/s00401-013-1108-7 [PubMed: 23543187]

26. Kuo SH, Wang J, Tate WJ, Pan MK, Kelly GC, Gutierrez J et al. (2017) Cerebellar pathology in early onset and late onset essential tremor. Cerebellum 16:473–482. 10.1007/s12311-016-0826-5 [PubMed: 27726094]

27. Lee PKC, Chatterjee D, Koeppen AH, Faust PL, Louis ED (2019) A quantitative study of empty baskets in essential tremor and other motor neurodegenerative diseases. JNEN 78:113–122. 10.1093/jnen/nly114

28. Lin CY, Louis ED, Faust PL, Koeppen AH, Vonsattel JP, Kuo SH (2014) Abnormal climbing fibre-Purkinje cell synaptic connections in the essential tremor cerebellum. Brain 137:3149–3159. 10.1093/brain/awu281 [PubMed: 25273997]

29. Louis ED (2010) Essential tremor: evolving clinicopathological concepts in an era of intensive post-mortem enquiry. Lancet Neurol 9:613–622. 10.1016/S1474-4422(10)70090-9 [PubMed: 20451458]

30. Louis ED, Babij R, Lee M, Cortes E, Vonsattel JP (2013) Quantification of cerebellar hemispheric purkinje cell linear density: 32 ET cases versus 16 controls. Mov Disord 28:1854–1859. 10.1002/mds.25629 [PubMed: 23925732]

31. Louis ED, Faust PL, Vonsattel JP, Honig LS, Rajput A, Rajput A et al. (2009) Torpedoes in Parkinson's disease, Alzheimer's disease, essential tremor, and control brains. Mov Disord 24:1600–1605. 10.1002/mds.22567 [PubMed: 19526585]

32. Louis ED, Faust PL, Vonsattel JP, Honig LS, Rajput A, Robinson CA et al. (2007) Neuropathological changes in essential tremor: 33 cases compared with 21 controls. Brain 130:3297–3307. 10.1093/brain/awm266 [PubMed: 18025031]

33. Louis ED, Kuo SH, Tate WJ, Kelly GC, Gutierrez J, Cortes EP et al. (2018) Heterotopic Purkinje cells: a comparative postmortem study of essential tremor and spinocerebellar ataxias 1, 2, 3, and 6. Cerebellum 17:104–110. 10.1007/s12311-017-0876-3 [PubMed: 28791574]

34. Louis ED, Kuo SH, Vonsattel JP, Faust PL (2014) Torpedo formation and Purkinje cell loss: modeling their relationship in cerebellar disease. Cerebellum 13:433–439. 10.1007/s12311-014-0556-5 [PubMed: 24590661]

35. Louis ED, Lee M, Babij R, Ma K, Cortes E, Vonsattel JP et al. (2014) Reduced Purkinje cell dendritic arborization and loss of dendritic spines in essential tremor. Brain 137:3142–3148. 10.1093/brain/awu314 [PubMed: 25367027]

36. Louis ED, Vonsattel JP, Honig LS, Ross GW, Lyons KE, Pahwa R (2006) Neuropathologic findings in essential tremor. Neurology 66:1756–1759 [PubMed: 16769958]

37. Ma X, Su W, Li S, Li C, Wang R, Chen M, Chen H (2018) Cerebellar atrophy in different subtypes of Parkinson's disease. J Neurol Sci 392:105–112. 10.1016/j.jns.2018.06.027 [PubMed: 30036781]

38. Mirra SS (1997) The CERAD neuropathology protocol and consensus recommendations for the postmortem diagnosis of Alzheimer's disease: a commentary. Neurobiol Aging 18:S91–S94 [PubMed: 9330994]

39. Paris-Robidas S, Brochu E, Sintes M, Emond V, Bousquet M, Vandal M et al. (2012) Defective dentate nucleus GABA receptors in essential tremor. Brain 135:105–116. 10.1093/brain/awr301 [PubMed: 22120148]

40. Prudente CN, Pardo CA, Xiao J, Hanfelt J, Hess EJ, Ledoux MS et al. (2013) Neuropathology of cervical dystonia. Exp Neurol 241:95–104. 10.1016/j.expneurol.2012.11.019 [PubMed: 23195594]

41. Samson M, Claassen DO (2017) Neurodegeneration and the cerebellum. Neurodegener Dis 17:155–165. 10.1159/000460818 [PubMed: 28463835]

42. Scherzed W, Brunt ER, Heinsen H, de Vos RA, Seidel K, Burk K et al. (2012) Pathoanatomy of cerebellar degeneration in spinocerebellar ataxia type 2 (SCA2) and type 3 (SCA3). Cerebellum 11:749–760. 10.1007/s12311-011-0340-8 [PubMed: 22198871]

43. Seidel K, Siswanto S, Brunt ER, den Dunnen W, Korf HW, Rub U (2012) Brain pathology of spinocerebellar ataxias. Acta Neuropathol 124:1–21. 10.1007/s00401-012-1000-x [PubMed: 22684686]

44. Shakkottai VG, Batla A, Bhatia K, Dauer WT, Dresel C, Niethammer M et al. (2017) Current opinions and areas of consensus on the role of the cerebellum in dystonia. Cerebellum 16:577–594. 10.1007/s12311-016-0825-6 [PubMed: 27734238]

45. Solodkin A, Gomez CM (2012) Spinocerebellar ataxia type 6. Handb Clin Neurol 103:461–473. 10.1016/B9780-444-51892-7.00029-2 [PubMed: 21827907]

46. Thal DR, Rub U, Orantes M, Braak H (2002) Phases of A betadeposition in the human brain and its relevance for the development of AD. Neurology 58:1791–1800 [PubMed: 12084879]

47. Wenning GK, Tison F, Ben Shlomo Y, Daniel SE, Quinn NP (1997) Multiple system atrophy: a review of 203 pathologically proven cases. Mov Disord 12:133–147. 10.1002/mds.870120203 [PubMed: 9087971]

48. Yu M, Ma K, Faust PL, Honig LS, Cortes E, Vonsattel JP et al. (2012) Increased number of Purkinje cell dendritic swellings in essential tremor. Eur J Neurol 19:625–630. 10.1111/j.1468-1331.2011.03598.x [PubMed: 22136494]
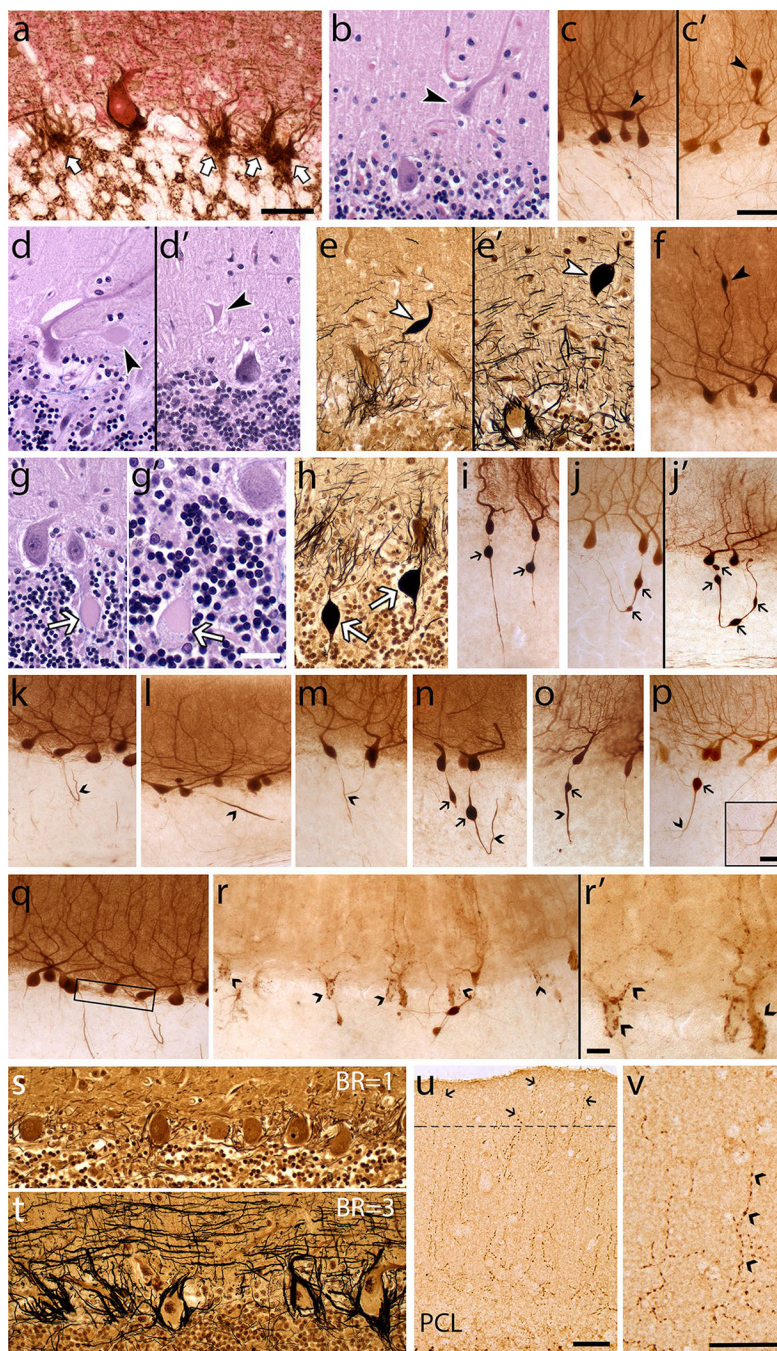
Fig. 1.
Morphologic metrics to characterize cerebellar pathology. Metrics are shown for each category of pathologic change (see Table 1). (1) PC loss, reflected by empty baskets in calbindinD$_{28k}$ (CB)-GAD immunostain (**a** arrows). Characteristic morphology of PCs with or without a nucleolus in LH&E stain is shown in (**g**) and (**g′**), respectively. (2) Heterotopic PCs (arrowheads) in LH&E stain (**b**) and CB immunostain [**c, c′**; note the PC body and primary dendrite oriented horizontally (**c**) or inverted (**c′**) relative to the underlying PC layer]. (3) PC dendritic changes (arrowheads), with dendrite swellings in LH&E stain (**d, d**

′), Bielschowsky stain (**e, e′**) and CB immunostain (**f**). (4) PC axonal changes, torpedoes (arrows) in LH&E stain (**g, g'** note granular blue material seen in the torpedo in **g′**), Bielschowsky stain (**h**) and CB immunostain (**i, j**), including axons with a single torpedo (**i**) or multiple torpedoes (**j, j′**). (5) PC axonal changes other than torpedoes in CB immunostain (carets), including recurrent collateral (**k**), thickened axon (**l**), axonal branching (**m**), recurrent collateral plexus (**q** boxed area), PC puncta (**r, r′**); see Suppl. Figure 1 for PC terminal sprout rating. (6) PC axonal changes, torpedo-associated in CB immunostain (carets; torpedoes noted by arrow), including torpedo with recurrent collateral (**n**), thickened axon (**o**), axonal branching (**p**). (7) Basket cell axonal hypertrophy, Bielschowsky stain (**s** basket rating = 1), (**t**, basket rating = 3). (8) Climbing fiber-PC synaptic changes, VGlut2 immunostain, including climbing fibers in outer 20% of molecular layer (**u** arrows), climbing fiber synaptic density (**v** carets label typical synaptic puncta). Scale bars **a, b, d, d′, e, e′, g, h, s, t, u** 50 μm (in panel **a**); **c, c′, f, j–r** 100 μm (in panel **c′**); **g′, p** (inset), **r′** 25 μm **v** 50 μm
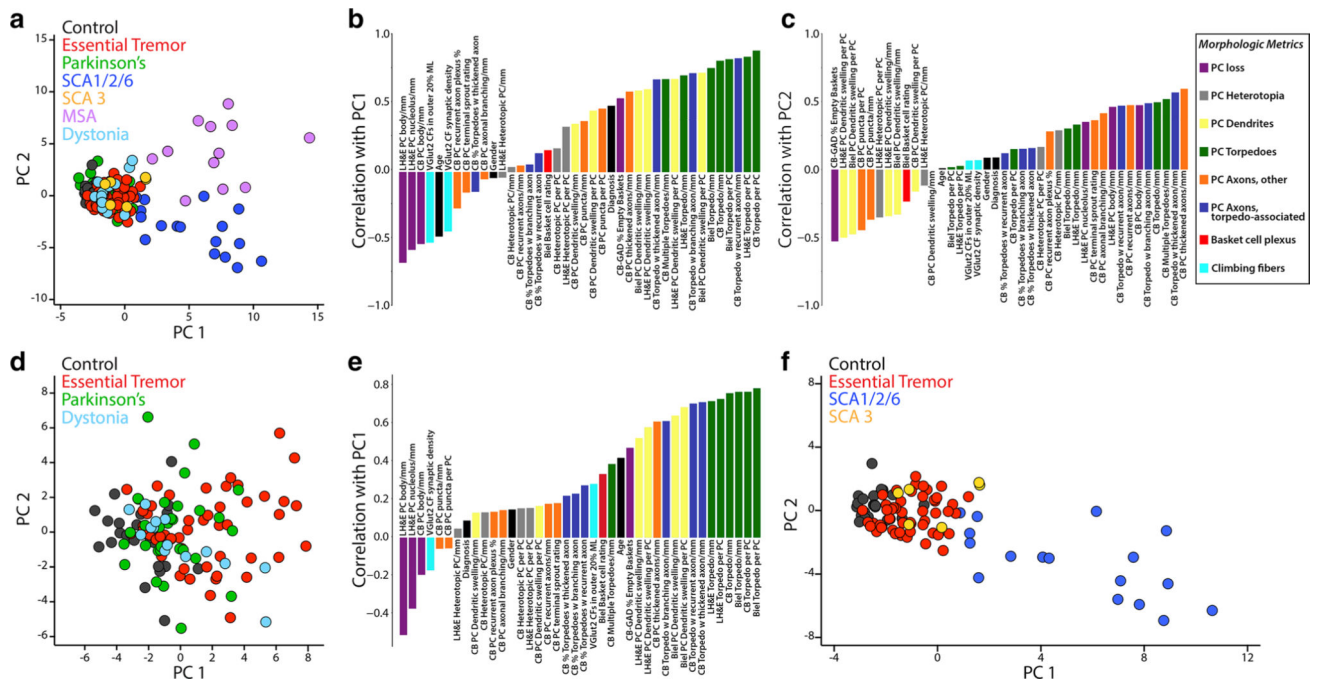
Fig. 2.

Principal component analyses of cerebellar morphologic metrics across diagnoses. Principal component analysis of the *z* scored raw data across all seven diagnostic categories (**a**) or across select diagnoses (**d, f**) shows how individual patients distribute across the two major axes of variation in the data, identifying distinct disease groupings. Each dot represents data from an individual patient. The bar graphs (**b, c, e**) show the Pearson's correlation between each morphologic metric and the first principal component (**b, e**) and the second principal component (**c**), and demonstrate disease-associated enrichment in varying observables. Each bar is labeled with the corresponding metric and color coded based on the eight categories of morphologic metrics, as indicated in the legend (see also Table 1) including Purkinje cell loss (purple), Purkinje cell heterotopia (gray), Purkinje cell dendrites (yellow), Purkinje cell torpedoes (green), Purkinje cell axons, other (orange), Purkinje cell axons, torpedo associated (blue), Basket cell plexus (red) and climbing fibers (light blue). *PC1* principal component 1, *PC2* principal component 2, *SCA* spinocerebellar ataxia, *MSA* multiple system atrophy, *PC* Purkinje cell
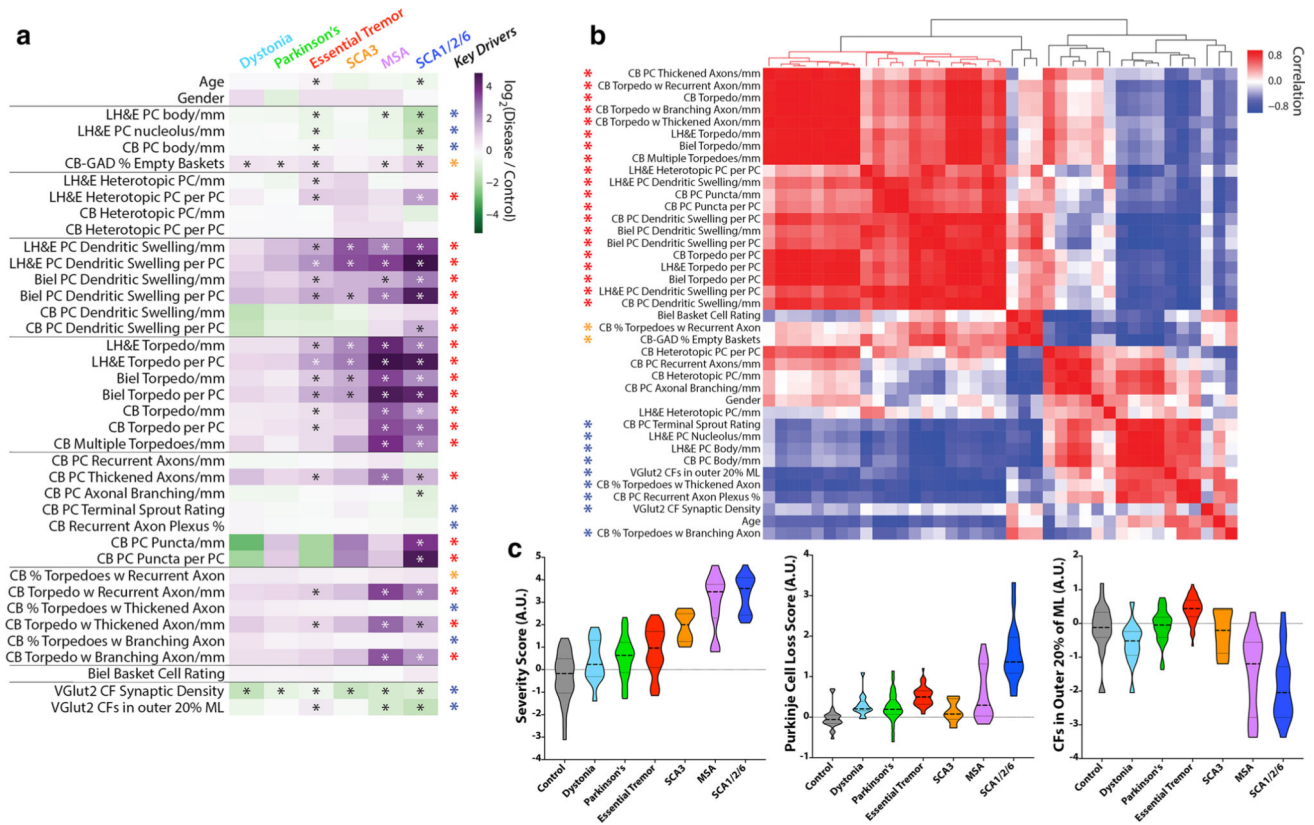
Fig. 3.

Differences in fold-change for each metric across diseases and key pathologic drivers. **a** Metrics (rows) and diagnoses (columns) are shown. Each cell in the heatmap is the average log$_2$-fold-change (disease vs. control) for each metric. The scale ranges from dark purple (high relative to control) to dark green (low relative to control). Elements with an asterisk indicate a statistically significant difference vs. controls (Mann–Whitney test, p values corrected for false discovery by Benjamini–Hochberg method; *FDR < 0.01). **b** Hierarchical clustering of the correlation coefficients between all pairwise combinations of metrics, with colored scale of red (positive correlation), white (no correlation) and blue (negative correlation). Prominent positively correlated (red and orange asterisks) or negatively correlated (blue asterisk) observables drive many of the significant differences across disease categories, and are designated as "*Key Drivers*" in **a**. **c** Three scores were computed across disease categories by combining the average fold-change (disease/control) for selected metrics and plotted on a log-transformed scale, including a "Severity Score" (large block of 20 positively correlated red metrics in panel b), a "Purkinje Cell Loss Score" (inverse Purkinje cell body, inverse Purkinje cell nucleolus and percent empty baskets), and a score reflecting climbing fibers (CFs) in the outer 20% of the molecular layer. Within each violin, the dashed line shows the median value and the dotted lines indicate outer quartiles in the data distribution
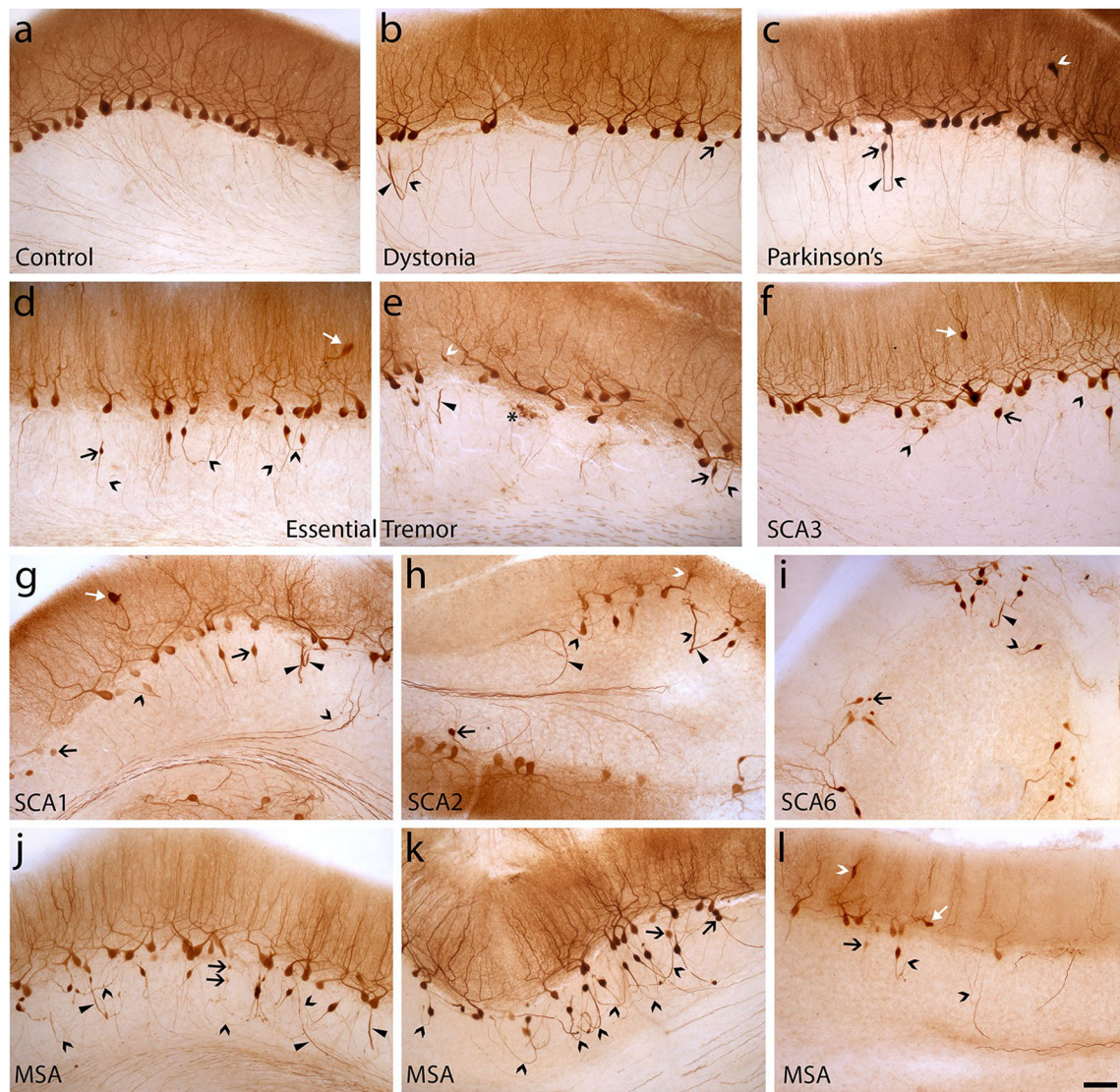
Fig. 4.

CalbindinD$_{28k}$ immunohistochemistry on 100-μm cerebellar neocortex sections across all seven diagnoses. Several categories of morphologic changes in Purkinje cells are identified, including cell body loss, heterotopia (white arrow, **d, f, g, l**), dendrite swelling (white caret, **c, e, h, l**), and axonal changes including torpedoes (large black arrow, **b–l**), thickened axons (arrowhead, **b, c, e, g–j**), recurrent collaterals (black caret, **b–l**), terminal axonal sprouting (asterisk, **e**). **a** Normal appearance of Purkinje cell dendrites, cell bodies and thin axon profiles in the granule cell layer in cerebellar cortex of a control. **b, c** Mild Purkinje cell axonal changes are seen in dystonia (**b**) and Parkinson's (**c**), with sparse thickened axons, recurrent collaterals and a torpedo. A dendrite swelling is present (**c**). **d, e** In Essential tremor, morphologic changes are more prominent, with greater loss of Purkinje cell bodies, heterotopia (**d**), dendrite swelling (**e**), thickened axon (**e**), several recurrent collaterals and torpedoes (**d, e**) and terminal axonal sprouting (**e**). (**f**) SCA3 with intermediate axonal changes including torpedoes and recurrent collaterals. A heterotopic Purkinje cell is present. **g–i** Spectrum of changes in SCA1/2/6: moderate to severe Purkinje cell body and dendrite

loss, abundant torpedoes, thickened axons and recurrent collaterals (many of which are associated with torpedoes). There is often significant loss of labeled axons in cerebellar folial white matter. When Purkinje cell loss is severe (e.g., **i**), the majority of cell bodies are associated with torpedoes. **j–k** Spectrum of changes in MSA: With milder Purkinje cell loss (**j**), there are numerous torpedoes, recurrent collaterals and thickened axons, but significant numbers of axons still project into folial white matter. With greater folial white matter degeneration (**k**), axons with torpedoes predominantly have recurrent collaterals, demonstrating prominent intracortical remodeling of Purkinje cell circuitry. In some MSA cases, Purkinje cell loss is severe, similar to that in severely affected SCAs. *SCA* spinocerebellar atrophy, *MSA* multiple system atrophy. Scale bar 100 μm, in (**l**)
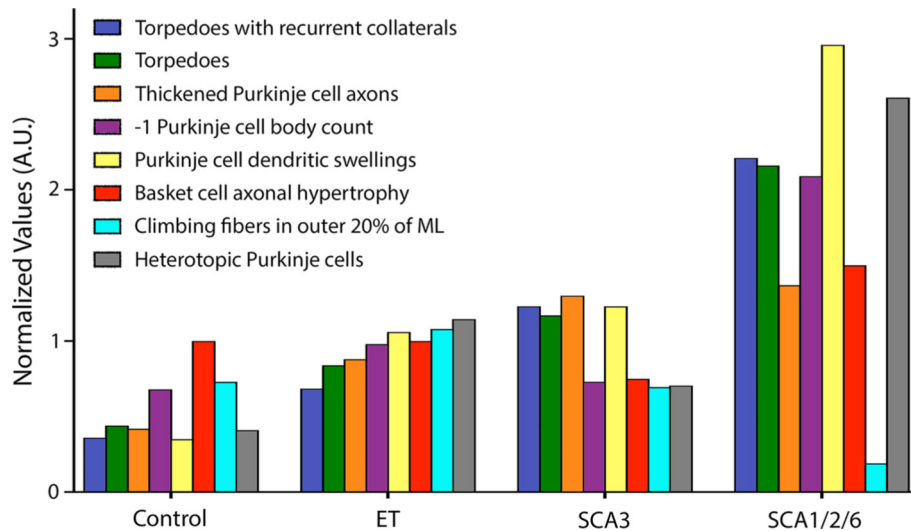
Fig. 5.
Skyline plot—patterns of degenerative changes across disorders. The median value for each of our eight core metrics are graphed in controls and essential tremor (ET) cases in comparison to primary disorders of cerebellar degeneration (i.e., SCAs). These include: torpedoes with recurrent collaterals/mm (blue bar, c albindinD$_{28k}$ immunostain), torpedoes/mm (green bar, c albindinD$_{28k}$ immunostain), thickened Purkinje cell axons/mm (orange bar, calbindinD$_{28k}$ immunostain), inverse (− 1) Purkinje cell body/mm (purple bar, LH&E stain), Purkinje cell dendritic swellings/mm (yellow bar, LH&E stain), basket cell axonal hypertrophy (red bar, Bielschowsky stain rating scale), Climbing fibers in outer 20% of ML (light blue bar, VGlut2 immunostain) and heterotopic Purkinje cells/mm (gray bar, LH&E stain). *ET* essential tremor, *SCA* spinocerebellar ataxia

Table 1

Category of pathological changes and metrics

Category of pathological change	Stain used	Metric	Published methods	Comment
PC cell loss	LH&E	PC body linear density (cells/mm)	See [11]	Adjusted for PC layer length
	LH&E	PC nucleolus linear density (cells/mm)	See [11]	Adjusted for PC layer length
	CB	PC body linear density (cells/mm)	See [30]	Adjusted for PC layer length
	CB-GAD	Percentage of empty baskets	See [27]	Indirect measure of PC loss
Heterotopic PCs	LH&E	Heterotopic PC linear density (cells/mm)	See [33]	Adjusted for PC layer length
	LH&E	Heterotopic PCs per PC	See [33]	Adjusted for the number of PCs
	CB	Heterotopic PC linear density (cells/mm)	See [33]	Adjusted for PC layer length
	CB	Heterotopic PCs per PC	See [33]	Adjusted for the number of PCs
PC dendritic changes	LH&E	PC dendritic swelling density (swellings/mm]	See [48]	Adjusted for PC layer length
	LH&E	PC dendritic swellings per PC	See [48]	Adjusted for the number of PCs
	Bielschowsky	PC dendritic swelling density (swellings/mm]	See [48]	Adjusts for PC layer length
	Bielschowsky	PC dendritic swellings per PC	See [48]	Adjusted for the number of PCs
	CB	PC dendritic swelling density (swellings/mm]	See [4]	Adjusted for PC layer length
	CB	PC dendritic swellings per PC	See [4]	Adjusted for the number of PCs
PC axonal changes (torpedoes)	LH&E	Torpedo linear density (torpedoes/mm)	See [31]	Adjusted for PC layer length
	LH&E	Torpedoes per PC	See [31]	Adjusted for the number of PCs
	Bielschowsky	Torpedo linear density (torpedoes/mm)	See [32]	Adjusted for PC layer length
	Bielschowsky	Torpedoes per PC	See [32]	Adjusted for the number of PCs
	CB	Torpedo linear density (torpedoes/mm)	See [4]	Adjusted for PC layer length
	CB	Torpedoes per PC	See [4]	Adjusted for the number of PCs
	CB	Mutliple ($\geq$ 2) torpedo density (multiple torpedoes/mm)	See [4]	Adjusted for PC layer length
PC axonal changes (other than torpedoes)	CB	PC axonal recurrent collaterals density (recurrent collaterals per mm)	See [4]	Adjusted for PC layer length
	CB	PC thickened axonal profiles (thickened axonal profiles per mm)	See [4]	Adjusted for PC layer length
	CB	PC axonal branching (branches per mm)	See [4]	Adjusted for PC layer length
	CB	PC terminal sprout rating	See Suppl. Figure 1.	
	CB	PC plexus percentage	See [4]	
	CB	PC puncta density (puncta per mm)	See Fig. 1.	Adjusted for PC layer length
	CB	PC puncta per PC	See Fig. 1.	Adjusted for the number of PCs

Category of pathological change	Stain used	Metric	Published methods	Comment
PC axonal changes (torpedo-associated)	CB	Percentage of torpedoes with axonal recurrent collaterals	See [4]	
	CB	Torpedoes with axonal recurrent collaterals (per mm)	See [4]	Adjusted for PC layer length
	CB	Percentage of torpedoes with thickened axons	See [4]	
	CB	Torpedoes with thickened axons (per mm)	See [4]	Adjusted for PC layer length
	CB	Percentage of torpedoes with branching axons	See [4]	
	CB	Torpedoes with branching axons (per mm)	See [4]	Adjusted for PC layer length
Basket cell axonal hypertrophy	Bielschowsky	Basket cell rating	See [4]	
Climbing fiber-PC synaptic changes	VGlut2	Climbing fiber synaptic density	See [28]	
	VGlut2	Percentage of climbing fibers in the outer 20% of the molecular layer	See [28]	

CB calbindin, *GAD* glutamic acid decarboxylase, *LH&E* Luxol fast blue/hematoxylin and eosin, *PC* Purkinje cell, *VGLut2* vesicular glutamate transporter type 2

Table 2

Demographic and pathological features by diagnosis

	Controls	Dystonia	PD	ET	SCA3	MSA	SCA1/2/6
N	25	14	29	50	6	15	17
Age at death (years)	75.3 ± 16.4 [80.0]	79.2 ± 9.2 [80.5] $p = 0.57$	78.0 ± 5.4 [79.0] $p = 0.92$	87.4 ± 6.3 [88.0] **$p = 0.001$**	55.5 ± 11.3 [59.0] **$p = 0.007$**	63.3 ± 9.3 [67.0] **$p = 0.01$**	58.9 ± 14.7 [63.0] **$p = 0.001$**
Male gender	15 (60.0%)	4 (28.6%) $p = 0.06$	22 (75.9%) $p = 0.21$	17 (34.0%) **$p = 0.03$**	2 (33.3) $p = 0.37$	5 (33.3%) $p = 0.10$	10 (58.8) $p = 0.94$
Brain weight (g)	1228 ± 176	1288 ± 100 $p = 0.31$	1342 ± 148 **$p = 0.01$**	1182 ± 135 $p = 0.21$	1235 ± 280 $p = 0.96$	1249 ± 97 $p = 0.72$	1159 ± 168 $p = 0.22$
Median (range) Thal stage for beta-amyloid[a]	0 (0–2)	1.5 (0–2) $p = 0.11$	2 (0–2) **$p < 0.001$**	1 (0–2) **$p = 0.003$**	NA	0 (0–2) $p = 0.95$	NA
Median (range) Braak Alzheimer's disease staging	1 (0–4)	2 (1–4) $p = 0.11$	3 (0–4) **$p < 0.001$**	2 (0–5) **$p = 0.001$**	NA	1 (0–4) $p = 0.52$	NA
Median (range) CERAD	0 (0–2)	0 (0–2) $p = 0.24$	1 (0–2) **$p = 0.016$**	1 (0–3) $p = 0.08$	NA	0 (0) $p = 0.09$	NA
Median postmortem interval (h)	4.5	NA	2.0 $p = 0.07$	2.3 **$p = 0.006$**	NA	0.9 **$p = 0.01$**	NA

Values are mean ± standard deviation [median] or number (percentage) unless otherwise specified. Statistical comparisons are with controls

Bolded values are statistically significant

Categorical or ordinal variables were compared using Chi-square tests. For continuous variables, we tested for normality using the Kolmogorov–Smirnov test. Continuous variables were compared using Student's t tests or, if not normally distributed, a non-parametric test (i.e., Mann–Whitney)

CERAD Consortium to Establish a Registry for Alzheimer's disease, *ET* essential tremor, *MSA* multiple system atrophy, *NA* not available, *PD* Parkinson's disease, *SCA* spinocerebellar ataxia

[a] Cerebellum negative for beta-amyloid plaques by immunohistochemistry in all cases

Table 3

Metrics in which a spectrum of pathological changes was observed

Category of pathological change	Stain	Metric	Spectrum of change observed
PC cell loss	LH&E	PC body linear density (cells/mm)[a]	
	LH&E	PC nucleolus linear density (cells/mm)	
	CB	PC body linear density (cells/mm)	
	CB-GAD	Percentage of empty baskets[a]	
Heterotopic PCs	LH&E	Heterotopic PC linear density (cells/mm)	
	LH&E	Heterotopic PCs per PC[a]	
	CB	Heterotopic PC linear density (cells/mm)	
	CB	Heterotopic PCs per PC	
PC dendritic changes	LH&E	PC dendritic swelling linear density (swellings/mm)	
	LH&E	PC dendritic swellings per PC	
	Bielschowsky	PC dendritic swelling linear density (swellings/mm)	
	Bielschowsky	PC dendritic swellings per PC[a]	
	CB	PC dendritic swelling linear density (swellings/mm)	
	CB	PC dendritic swellings per PC	
PC axonal changes (torpedoes)	LH&E	Torpedo linear density (torpedoes/mm)	
	LH&E	Torpedoes per PC[a]	
	Bielschowsky	Torpedo linear density (torpedoes/mm)	
	Bielschowsky	Torpedoes per PC	
	CB	Torpedo linear density (torpedoes/mm)	
	CB	Torpedoes per PC[a]	
	CB	Multiple torpedo density (multiple torpedoes/mm)	
PC axonal changes (other than torpedoes)	CB	PC axonal recurrent collaterals density (recurrent collaterals per mm)	
	CB	PC thickened axonal profiles density (thickened axonal profiles per mm)[a]	
	CB	PC axonal branching density (branches per mm)	
	CB	PC terminal sprout rating	
	CB	PC plexus percentage	

Category of pathological change	Stain	Metric	Spectrum of change observed
	CB	PC puncta density (PC with puncta per mm)	
	CB	PC puncta per PC	
PC axonal changes (torpedo-related)	CB	Percentage of torpedoes with axonal recurrent collaterals	
	CB	Torpedoes with axonal recurrent collaterals (per mm)[a]	
	CB	Percentage of torpedoes with thickened axons	
	CB	Torpedoes with thickened axons (per mm)	
	CB	Percentage of torpedoes with branching axons	
	CB	Torpedoes with branching axons (per mm)	
Basket cell axonal hypertrophy	Bielschowsky	Basket cell rating[a]	
Climbing fiber-PC synaptic changes	VGlut2	Climbing fiber synaptic density in molecular layer	
	VGlut2	Number of climbing fibers in the outer 20% of the molecular layer[a]	

= a spectrum of change was observed, with ET generally at the low end and SCA1/2/6 or MSA at the high end of severity

CB calbindin, *GAD* glutamic acid decarboxylase, *LH&E* Luxol fast blue/hematoxylin and eosin, *PC* Purkinje cell, *VGLut2* vesicular glutamate transporter type 2

[a]10 metrics in the ET neuropathological score